Calculation of line shapes in double-resonance optical pumping

Heung-Ryoul Noh[1,*] and Han Seb Moon[2,†]
[1]*Department of Physics, Chonnam National University, Gwangju 500-757, Korea*
[2]*Department of Physics, Pusan National University, Busan 609-735, Korea*
(Received 30 April 2009; published 14 August 2009)

A theoretical study on double-resonance optical pumping for the transitions $5S_{1/2}$-$5P_{3/2}$-$4D_{3/2,5/2}$ of ^{87}Rb atoms is presented. The full-density-matrix equations in the presence the probe and the coupling laser beams for all relevant magnetic sublevels of the hyperfine levels were solved numerically, and the absorption of a probe beam was calculated as a function of the detuning of the coupling beam. The calculated results were compared with experimental data, and they showed an excellent agreement. The results were also compared with the approximate results calculated when the coherence between the ground and the highest excited levels was neglected. We found that the dominant operating mechanism for double-resonance signals was the optical pumping rather than the two-photon coherence, although the latter affected the signals significantly.

DOI: 10.1103/PhysRevA.80.022509 PACS number(s): 32.30.−r, 32.70.Jz, 32.80.Xx

I. INTRODUCTION

High-resolution spectroscopy has seen a widespread use in applications such as laser frequency stabilization, laser cooling, atomic clocks, and optical frequency references [1]. Doppler-free spectroscopy in the transitions between excited states has been used in high-resolution spectroscopy, laser frequency stabilization, and frequency references in optical communication [2–8]. In order to obtain a highly resolved spectrum for the transition from one excited state to another excited state, various optical pumping methods, such as the optical-optical double-resonance (OODR) technique, have successfully used a laser as a pumping light source with a narrow linewidth in atomic spectroscopy [1–8].

Recently, Moon *et al.* used the double-resonance optical pumping (DROP) technique to observe a well-resolved spectrum with a high signal-to-noise ratio (SNR) in the transition between excited states [9–12]. The DROP method improved the SNR of this spectrum remarkably, by nearly a factor of 10 in comparison with a conventional OODR method [9]. The group investigated the influence of the polarization combinations, the power, and the alignment of lasers on the DROP of a $5S_{1/2}$-$5P_{3/2}$-$4D_{3/2,5/2}$ ladder-type atomic system to room-temperature ^{87}Rb atoms (see Fig. 1) in a vapor cell and interpreted this DROP spectrum by considering the two-photon transition probability and optical pumping [10]. They also applied the DROP method to the frequency stabilization of a laser diode in the 1.5 μm region and determined the hyperfine constants of the $4D_{5/2}$ state for ^{87}Rb atoms [9,11].

The DROP is performed by optical pumping from one of the hyperfine levels of the ground state to another hyperfine level of the ground state through the excited state and the intermediate states in the ladder-type atomic system [9,10]. Although the DROP spectrum is explained by considering the two-photon transition probability and optical pumping [10], it is not easy to predict both the correct DROP spectrum and also the power dependence of the $D_{5/2}$ state, because it is not based on rigorous theory for the real atomic system with a two-photon coherence. In this paper, we perform a theoretical study of the DROP spectra by solving the density-matrix equation for multilevel atoms in the $5S_{1/2}$-$5P_{3/2}$-$4D_{3/2,5/2}$ transition of ^{87}Rb atoms. In Sec. II, we describe our method for calculating the DROP spectra. We simulate the DROP spectra as a function of the power of the pump laser, which affects the linewidths and the magnitude of the DROP spectra. In Sec. III, the calculated spectra are compared with experimental results. In particular, by comparing the spectra simulated via the rate equation with those simulated with the density-matrix equation, we investigate in detail the optical pumping effect and the two-photon coherence effect in the DROP spectra. We simulate the DROP spectra as a function of the power of the pump laser, which affects the linewidths and the magnitude of the DROP spectra. The final section summarizes the results.

II. THEORY

The resonance wavelength (λ_1) for the $5S_{1/2}$-$5P_{3/2}$ probe line is 780 nm, while the resonant wavelength (λ_2) for the

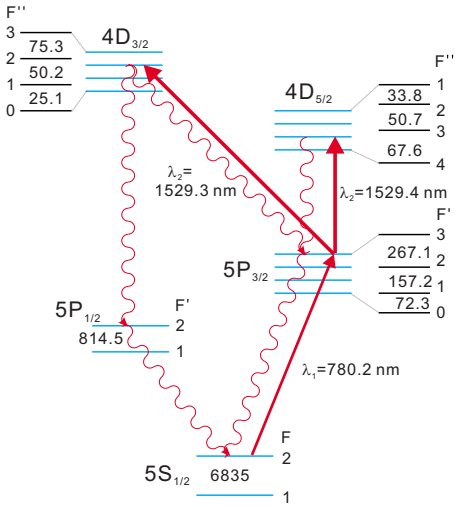

FIG. 1. (Color online) Energy-level diagram for DROP: the frequencies are shown in units of MHz.

*hrnoh@chonnam.ac.kr
†hsmoon@pusan.ac.kr

$5P_{3/2}$-$4D_{3/2,5/2}$ coupling line is 1529 nm. The probe laser frequency is locked at the $5S_{1/2}(F=2)$-$5P_{3/2}(F'=3)$ transition line, whereas the coupling laser is scanned around the $5P_{3/2}(F'=3)$-$4D_{3/2,5/2}$ transition lines. The decay rates of the $5P_{3/2}$ and the $4D_{5/2}$ states are approximately $\Gamma_1=2\pi\times 6$ MHz [13] and $\Gamma_2=2\pi\times 2$ MHz [5], respectively. The frequency intervals of the $4D_{3/2,5/2}$ states are derived from hyperfine-structure constants given in Ref. [14]. We consider only the π transition ($\Delta m=0$) for the $5S_{1/2}$-$5P_{3/2}$ transition and the $5P_{3/2}$-$4D_{3/2,5/2}$ transition.

The internal dynamics of the ^{87}Rb atom is described by the following density-matrix equation [15]:

$$\frac{\partial\rho}{\partial t}=-\frac{i}{\hbar}[H_0+V_1+V_2,\rho]+\dot{\rho}_{\rm sp}\equiv Q^{(1)}, \tag{1}$$

where ρ is the density-matrix operator. The atomic Hamiltonian H_0 is given by

$$H_0=\sum_{F''=1}^{4}\hbar(\omega_{10}+\omega_{20}+\Delta_4^{F''})\sum_{m=-F''}^{F''}|F'',m\rangle\langle F'',m| + \sum_{F'=1}^{3}\hbar(\omega_{10}+\Delta_{F'}^{3})\sum_{m=-F'}^{F'}|F',m\rangle\langle F',m|, \tag{2}$$

where ω_{10} and ω_{20} are the resonant frequencies for the transitions $5S_{1/2}(F=2)$-$5P_{3/2}(F'=3)$ and $5P_{3/2}(F'=3)$-$5D_{5/2}(F''=4)$, respectively. The energy spacing between the hyperfine levels in each fine-structure level is given by $\hbar\Delta_\mu^\nu=E_\nu-E_\mu$. F'', F', and F denote the angular momenta of the hyperfine levels for the states $4D_{3/2,5/2}$, $5P_{3/2}$, and $5S_{1/2}$, respectively. For brevity, these fine-structure levels are represented by the notations F'', F', and F.

In Eq. (1), V_1 and V_2 are the interaction Hamiltonians with the probe and with the coupling beam, respectively. Because we are considering the probe and the coupling beam as linearly polarized, the interaction Hamiltonians are given by [15]

$$V_1=\frac{1}{2}\hbar\Omega_1\sum_{F'=1}^{3}\sum_{m=-2}^{2}C_{F=2,m}^{F',m}e^{-i\omega_1 t}|F',m\rangle\langle F=2,m|+\text{H.c.}, \tag{3}$$

$$V_2=\frac{1}{2}\hbar\Omega_2\sum_{F''=F'-1}^{F'+1}\sum_{F'=1}^{3}\sum_{m=-F'}^{F'}C_{F',m}^{F'',m}e^{-i\omega_2 t}|F'',m\rangle\langle F',m|+\text{H.c.}, \tag{4}$$

where the Rabi frequencies and the saturation intensities are

$$\Omega_i=\Gamma_i\left(\frac{I_i}{2I_{S_i}}\right)^{1/2},\quad I_{S_i}=\frac{\pi hc\Gamma_i}{3\lambda_i}, \tag{5}$$

with $i=1,2$. ω_1 and ω_2 are the angular frequencies of the probe and the coupling lasers, respectively. The normalized transition coefficient is given by [16]

$$C_{F_g,m_g}^{F_e,m_e}=(-1)^{2F_e+I+J_g+J_e+L_g+S+m_{F_g}+1}\times\sqrt{(2L_e+1)(2J_e+1)(2J_g+1)(2F_e+1)(2F_g+1)}\times\begin{Bmatrix}L_g & L_e & 1\\ J_e & J_g & S\end{Bmatrix}\begin{Bmatrix}J_g & J_e & 1\\ F_e & F_g & I\end{Bmatrix}\times\begin{pmatrix}F_e & 1 & F_g\\ m_e & m_g-m_e & -m_g\end{pmatrix},$$

where L, S, and I represent the orbital, the electron-spin, and the nuclear-spin angular momenta, respectively. $(\cdots)$ and $\{\cdots\}$ denote the $3J$ and the $6J$ symbols, respectively. In calculating the DROP signals for the $5S_{1/2}$-$5P_{3/2}$-$4D_{3/2}$ transition, the decay from the state $4D_{3/2}$ to $5S_{1/2}$ via the state $5P_{1/2}$ should be taken into account. The matrix elements of the operator $\dot{\rho}_{\rm sp}$ describing the spontaneous emissions are presented in the Appendix.

Since the matrix elements (ρ_{ij}) possess fast time dependence, these are transformed to the slowly varying elements (σ_{ij}) by the relation $\rho_{ij}=e^{ic_{ij}t}\sigma_{ij}$ [15], where

$$c_{ij}=\begin{cases}-\omega_2, & (i,j)\in(F'',F')\\ -\omega_1-\omega_2, & (i,j)\in(F'',F)\\ \omega_2, & (i,j)\in(F',F'')\\ -\omega_1, & (i,j)\in(F',F)\\ \omega_1+\omega_2, & (i,j)\in(F,F'')\\ \omega_1, & (i,j)\in(F,F')\\ 0, & (i,j)\in(F'',F''),(F',F'),(F,F).\end{cases}$$

In the construction of the matrices, the bases are assumed to be aligned from the upper to the lower levels. Then Eq. (1) becomes

$$\dot{\sigma}_{ij}=e^{-ic_{ij}t}Q_{ij}^{(1)}-ic_{ij}\sigma_{ij}. \tag{6}$$

Because the right-hand side of Eq. (6) has no explicit time dependence, Eq. (6) generates the first-order differential equations. Equation (6) is dependent on the velocity of the atom via the relations for the laser detunings,

$$\delta_1=\omega_1-\omega_{10}=-k_1v,$$

$$\delta_2=\omega_2-\omega_{20}=\delta-k_2v,$$

where $k_1=2\pi/\lambda_1$, $k_2=2\pi/\lambda_2$, and δ is the laser frequency relative to the transition $5P_{3/2}(F'=3)$-$4D_{5/2}(F''=4)$ or $5P_{3/2}(F'=3)$-$4D_{3/2}(F''=2)$.

The absorption coefficient, averaged over the Maxwell-Boltzmann velocity distribution, at a given time t is given by [17]

$$\alpha(t)=\frac{3\lambda_1^2}{2\pi}\frac{\Gamma_1}{\Omega_1}\frac{N_{\rm at}}{\sqrt{\pi}u}\int_{-\infty}^{\infty}dv\ e^{-(v/u)^2}\times\sum_{F'=1}^{3}\sum_{m=-2}^{2}C_{F=2,m}^{F',m}\,\text{Im}\langle F=2,m|\sigma|F',m\rangle, \tag{7}$$

where $u=(2k_BT/M)^{1/2}$ is the most probable speed (T is the temperature of the vapor cell and M is the mass of a ^{87}Rb atom), N_{at} is the atomic density, and the matrix elements are dependent on time and v. If we consider the fact that the atoms have a chance to interact with the laser light while passing through the laser light, the measured transmission is given by

$$\alpha = \frac{1}{t_{av}} \int_0^{t_{av}} \alpha(t) dt, \tag{8}$$

where the average transit time is given by $t_{av}=(\sqrt{\pi}/2)d/u$, with d as the diameter of the laser beam [18]. Equation (8) is the final result for the absorption coefficient, and the transmission can now be obtained by $\exp(-\alpha l)$ with l as the length of the cell. We also study the effect of the coherences between the ground ($5S_{1/2}$) and the highly excited levels ($4D_{3/2,5/2}$). In this case, the matrix elements σ_{ij} between the states $5S_{1/2}$ and $4D_{3/2,5/2}$ in Eq. (6) are set to zero.

III. COMPARISON WITH EXPERIMENTAL RESULTS

We now present a comparison of the simulation with the experimental results. For the experimental data, we used the data presented in the previous report [10]. Because a detailed explanation of the experimental procedure was presented in that report [10], we summarize the experimental method only briefly. Two external cavity diode lasers were used for the probe and the coupling lasers. Both beams were linearly polarized and propagated codirectionally. While the probe beam ($\lambda_1=780$ nm) was locked to $5S_{1/2}$-$5P_{3/2}$, the coupling beam ($\lambda_2=1529$ nm) was scanned over the entire range of the excited states for the transition lines $5P_{3/2}$-$4D_{3/2,5/2}$. The diameter of the probe and the coupling beams was adjusted with irises to be approximately 1.5 mm. The rubidium cell, which had a length of 10 cm, was kept at room temperature. To eliminate the effects of the terrestrial magnetic field, the rubidium cell was wrapped with μ-metal sheets.

Figures 2(a) and 2(b) show the DROP spectra for the transitions $5S_{1/2}$-$5P_{3/2}$-$4D_{3/2}$ and $5S_{1/2}$-$5P_{3/2}$-$4D_{5/2}$, respectively. The power of the probe laser beam was 78 μW, while that of the coupling laser was varied: it was 1.33 (upper trace) and 0.14 mW (lower trace) in Fig. 2(a), and it was 0.67 (upper trace) and 0.23 mW (lower trace) in Fig. 2(b). In Fig. 2, the experimental spectra were superimposed over the calculated spectra. We present two kinds of calculated results: one is an exactly calculated result that includes all the coherences, as described in the preceding section, and the other is an approximate result that neglected the two-photon coherences between the ground ($5S_{1/2}$) and the highest excited ($4D_{3/2}$ or $4D_{5/2}$) levels. In Fig. 2 one can see a very good agreement between the experimental and the exactly calculated results. In contrast, there are discrepancies between the experimental and the approximately calculated results. In particular, the width for the approximate results is ~20% larger than for the experimental results. Although the overall line shape of the DROP signal was influenced mostly by the optical pumping, we can see that the height and the width of the DROP signal are to a certain extent dependent on the two-photon coherence between the ground and the highly excited levels.

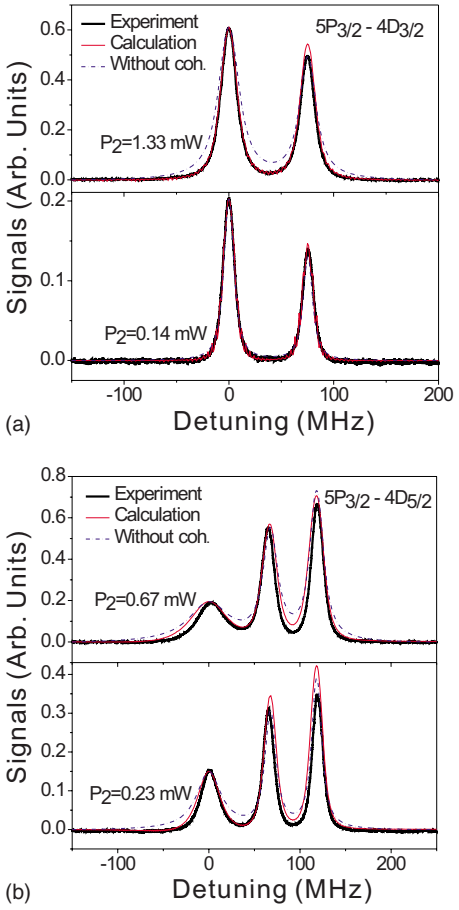

FIG. 2. (Color online) Comparison between the experimental and the calculated results for the transitions (a) $5S_{1/2}$-$5P_{3/2}$-$4D_{3/2}$ and (b) $5S_{1/2}$-$5P_{3/2}$-$4D_{5/2}$.

Although the effect of the two-photon coherence is weaker than that of optical pumping, it is possible to discriminate the effect of the coherence and the effect of the optical pumping in the DROP spectra by calculation. In particular, the relative amplitude of two peaks ($F'=3\rightarrow F''=2$) and ($F'=3\rightarrow F''=3$) in the $5S_{1/2}$-$5P_{3/2}$-$4D_{3/2}$ transition was different from the calculated result by considering the two-photon transition probability [10]. In this paper, the experimental result can be predicted from the calculation by taking into account the decay from the state $4D_{3/2}$ to $5S_{1/2}$ via the state $5P_{1/2}$ as well as the state $5P_{3/2}$.

Figure 3 shows the coupling-laser-intensity dependence of the DROP spectra. The calculated DROP spectra for the transitions $5S_{1/2}$-$5P_{3/2}$-$4D_{3/2}$ and $5S_{1/2}$-$5P_{3/2}$-$4D_{5/2}$ are presented in Figs. 3(a) and 3(b), respectively. For the calculations whose results are shown in Figs. 3(a) and 3(b), the intensity of the probe laser was set to 50 W/m^2, whereas the intensities of the coupling laser beam were set to 5, 10, 50, 100, 500, and 1000 W/m^2 with the resulting lines in the figures ordered from the bottom to the top of each figure. As noted in the previous report [10], the DROP spectra for the $4D_{3/2}$ levels show similar behavior for different laser intensities. As the intensity of the coupling laser beam increases, the line

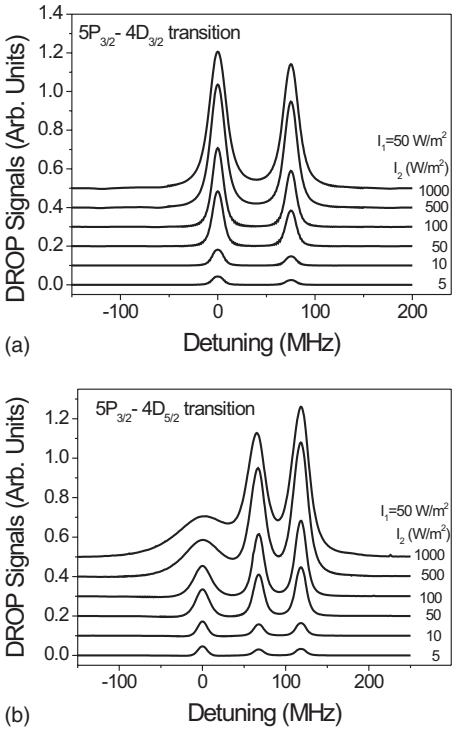

FIG. 3. The DROP spectra with different coupling laser intensities for the transitions (a) $5S_{1/2}$-$5P_{3/2}$-$4D_{3/2}$ and (b) $5S_{1/2}$-$5P_{3/2}$-$4D_{5/2}$.

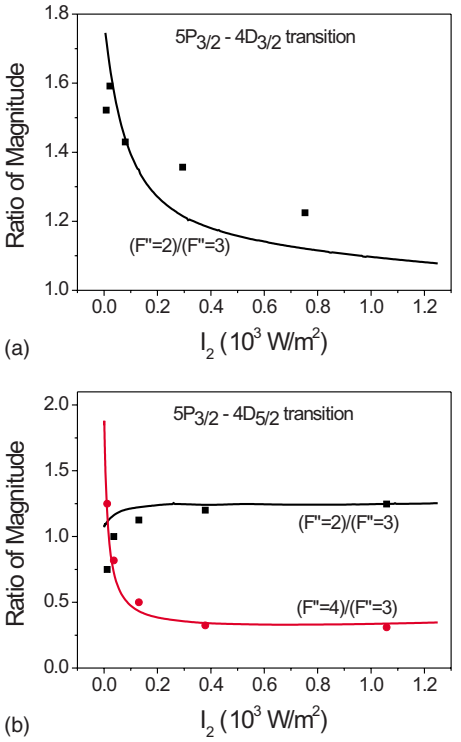

FIG. 4. (Color online) Magnitude of the DROP signals as a function of the coupling laser intensity for the transitions (a) $5S_{1/2}$-$5P_{3/2}$-$4D_{3/2}$ and (b) $5S_{1/2}$-$5P_{3/2}$-$4D_{5/2}$.

shape becomes wider due to the power-broadening effect.

In contrast, as can be seen in Fig. 3(b), the DROP spectra for the $4D_{5/2}$ level exhibit dramatic variations as the laser intensity changes. When the coupling laser intensity is weaker than ~ 10 W/m^2, the amplitude for the $5P_{3/2}(F'=3)$-$4D_{5/2}(F''=4)$ transition is larger than other signals for the $4D_{5/2}(F''=3)$ or the $4D_{5/2}(F''=2)$ level. However, as the laser intensity increases, the transmission amplitude becomes weaker than the other signals. This can be attributed to the strong cycling transition between the $5P_{3/2}(F'=3)$ and the $4D_{5/2}(F''=4)$ levels. When the coupling laser intensity is weak, since the strength of the cycling transition line $5P_{3/2}(F'=3)$-$4D_{5/2}(F''=4)$ is very strong despite the nonexistence of optical pumping channels other than $5P_{3/2}(F'=3)$, the population of the intermediate state $(5P_{3/2})$ is easily depleted for that cycling transition line, resulting in a large DROP signal. However, when the intensity of the coupling laser is strong, the effect of the optical pumping for other transitions exceeds the saturation effect of the cycling transition line. Therefore, we can observe large DROP signals for the $5P_{3/2}(F'=3)$-$4D_{5/2}(F''=3)$ or the $4D_{5/2}(F''=2)$ transition at high coupling laser intensities.

Figure 4 shows a comparison between the experimental and the calculated results for the magnitude of the DROP signals as a function of the intensity of the coupling laser. Figures 4(a) and 4(b) show the results for the transitions $5S_{1/2}$-$5P_{3/2}$-$4D_{3/2}$ and $5S_{1/2}$-$5P_{3/2}$-$4D_{5/2}$, respectively. In Fig. 4, the intensity of the probe laser was 44 W/m^2. In Fig. 4(a) [Fig. 4(b)], the magnitude was normalized to that for $4D_{3/2}(F''=3)$ $[4D_{5/2}(F''=3)]$. One can observe a good agreement between the calculated and the experimental results.

IV. CONCLUSIONS

In this paper, we have described a theoretical study of DROP spectra for ^{87}Rb atoms. Our theoretical work is able to produce accurate DROP spectra, including the all-hyperfine components of the $5S_{1/2}$-$5P_{3/2}$-$4D_{3/2,5/2}$ transition of ^{87}Rb atoms under all experimental conditions for laser intensities and diameters. We calculated the DROP spectra as a function of the power of the pump laser, which affected the linewidths and the magnitude of the DROP spectra. The calculated spectra were compared with the experimental results. In particular, comparing the spectra calculated without considering the two-photon coherences between the ground and the highly excited levels with the spectra derived from the density-matrix equation, we found that optical pumping was the dominant operating mechanism although the two-photon coherence also influenced the DROP spectra, particularly the width of the spectra. A theoretical study of the dependence of DROP signals on the various combinations of polarizations of the probe and the coupling laser is currently underway. It would be interesting to investigate DROP signals in copropagating and counterpropagating schemes and using other coupling transition wavelength.

ACKNOWLEDGMENTS

This work was supported by the Korea Research Foundation Grant funded by the Korean Government (Contract No. KRF-2008-313-C00355). Also, this work was supported by the Korea Science and Engineering Foundation (KOSEF)

grant funded by the Korean government (MOST) (Contract No. R01-2007-000-11636-0).

APPENDIX

The matrix elements describing the spontaneous emissions for the transition $5S_{1/2}$-$5P_{3/2}$-$4D_{5/2,3/2}$ are given by the following. For simplicity, the angular momenta F'', F', F, and $\tilde{F}$ denote the states $4D_{5/2,3/2}$, $5P_{3/2}$, $5S_{1/2}$, and $5P_{1/2}$, respectively,

$$\langle \mu, m_\mu | \dot{\rho}_{\mathrm{sp}} | \nu, m_\nu \rangle = -R_{J''}(\Gamma_1, \Gamma_2) \langle \mu, m_\mu | \rho | \nu, m_\nu \rangle, \quad \text{(A1)}$$

where

$$R_{5/2}(\Gamma_1,\Gamma_2) = \begin{cases} \Gamma_2, & (\mu,\nu) \in (F'',F'') \\ (\Gamma_1+\Gamma_2)/2, & (\mu,\nu) \in (F'',F') \\ \Gamma_2/2, & (\mu,\nu=2) \in (F'',F) \\ \Gamma_1/2, & (\mu,\nu=2) \in (F',F), \end{cases}$$

$$R_{3/2}(\Gamma_1,\Gamma_2) = \begin{cases} \Gamma_2, & (\mu,\nu) \in (F'',F'') \\ (\Gamma_1+\Gamma_2/6)/2, & (\mu,\nu) \in (F'',F') \\ \Gamma_2/12, & (\mu,\nu=2) \in (F'',F) \\ \Gamma_1/2, & (\mu,\nu=2) \in (F',F), \end{cases}$$

$$\begin{aligned} &\langle F', m_1 | \dot{\rho}_{\mathrm{sp}} | F', m_2 \rangle \\ &\quad = -\Gamma_1 \langle F', m_1 | \rho | F', m_2 \rangle \\ &\qquad + \Gamma_2 \sum_{F''=F'-1}^{F'+1} \sum_{q=-1}^{1} C_{F',m_1}^{F'',m_1+q} C_{F',m_2}^{F'',m_2+q} \\ &\qquad \times \langle F'', m_1+q | \rho | F'', m_2+q \rangle, \quad \text{for } F' = 0,1,2,3. \end{aligned} \quad \text{(A2)}$$

For the transition $5S_{1/2}$-$5P_{3/2}$-$4D_{5/2}$,

$$\begin{aligned} &\langle F=2, m_1 | \dot{\rho}_{\mathrm{sp}} | F=2, m_2 \rangle \\ &\quad = \Gamma_1 \sum_{F'=1}^{3} \sum_{q=-1}^{1} C_{F=2,m_1}^{F',m_1+q} C_{F=2,m_2}^{F',m_2+q} \langle F', m_1+q | \rho | F', m_2+q \rangle. \end{aligned} \quad \text{(A3)}$$

For the transition $5S_{1/2}$-$5P_{3/2}$-$4D_{3/2}$,

$$\begin{aligned} &\langle F=2, m_1 | \dot{\rho}_{\mathrm{sp}} | F=2, m_2 \rangle \\ &\quad = \Gamma_1 \sum_{F'=1}^{3} \sum_{q=-1}^{1} C_{F=2,m_1}^{F',m_1+q} C_{F=2,m_2}^{F',m_2+q} \langle F', m_1+q | \rho | F', m_2+q \rangle \\ &\qquad + \Gamma_1 \sum_{\tilde{F}=1}^{2} \sum_{q=-1}^{1} C_{F=2,m_1}^{\tilde{F},m_1+q} C_{F=2,m_2}^{\tilde{F},m_2+q} \langle \tilde{F}, m_1+q | \rho | \tilde{F}, m_2+q \rangle, \end{aligned} \quad \text{(A4)}$$

$$(\dot{\rho}_{\mathrm{sp}})_{ij} = (\dot{\rho}_{\mathrm{sp}})_{ji}, \quad \text{for } i \neq j. \quad \text{(A5)}$$

[1] W. Demtröder, *Laser Spectroscopy* (Springer, Berlin, 2003).
[2] J. Brossel and R. Bitter, Phys. Rev. **86**, 308 (1952).
[3] D. T. Vituccio, O. Golonzka, and W. E. Ernst, J. Mol. Spectrosc. **184**, 237 (1997).
[4] H. Sasada, IEEE Photonics Technol. Lett. **4**, 1307 (1992).
[5] M. Breton, N. Cyr, P. Tremblay, M. Têtu, and R. Boucher, IEEE Trans. Instrum. Meas. **42**, 162 (1993).
[6] S. L. Gilbert, Proc. SPIE **1837**, 146 (1993).
[7] M. Breton, P. Tremblay, N. Cyr, C. Julien, M. Têtu, and B. Villeneuve, Proc. SPIE **1837**, 134 (1993).
[8] M. Breton, P. Tremblay, C. Julien, N. Cyr, M. Têtu, and C. Latrasse, IEEE Trans. Instrum. Meas. **44**, 162 (1995).
[9] H. S. Moon, W. K. Lee, L. Lee, and J. B. Kim, Appl. Phys. Lett. **85**, 3965 (2004).
[10] H. S. Moon, L. Lee, and J. B. Kim, J. Opt. Soc. Am. B **24**, 2157 (2007).
[11] W. Lee, H. S. Moon, and H. S. Suh, Opt. Lett. **32**, 2810 (2007).
[12] H. S. Moon, L. Lee, and J. B. Kim, Opt. Express **16**, 12163 (2008).
[13] P. Siddons, C. S. Adams, C. Ge, and I. G. Hughes, J. Phys. B **41**, 155004 (2008).
[14] E. Arimondo, M. Inguscio, and P. Violino, Rev. Mod. Phys. **49**, 31 (1977).
[15] C. Cohen-Tannoudji, J. Dupont-Roc, and G. Grynberg, *Atom-Photon Interactions: Basic Processes and Applications* (Wiley, New York, 1992).
[16] A. R. Edmonds, *Angular Momentum in Quantum Mechanics* (Princeton University Press, Princeton, 1960).
[17] D. Meschede, *Optics, Light and Lasers* (Wiley-VCH, Weinheim, 2007).
[18] J. Sagle, R. K. Namiotka, and J. Huennekens, J. Phys. B **29**, 2629 (1996).